Title

Preservation of erniettomorph fossils in clay-rich siliciclastic deposits from the Ediacaran Wood Canyon Formation, Nevada

Journal

Interface Focus, 10(4)

ISSN

2042-8898

Authors

Hall, JG
Smith, EF
Tamura, N
et al.

Publication Date

2020-08-06

DOI

10.1098/rsfs.2020.0012

Peer reviewed

Preservation of erniettomorph fossils in clay-rich mass flow deposits from the Ediacaran Wood Canyon Formation, Nevada

Hall, J. G.[1]; Smith, E. F.[2]; Tamura, N.[3]; Fakra, S.C.[3]; Bosak, T.[1]
[1]Department of Earth, Atmospheric, and Planetary Sciences, Massachusetts Institute of Technology, Cambridge, United States
[2]Department of Earth and Planetary Sciences, Johns Hopkins University, Baltimore, United States
[3]Advanced Light Source, Lawrence Berkeley National Laboratory, Berkeley, United States

Key words: Ediacaran, cast and mold, erniettomorphs, taphonomy, clay minerals

Abstract:

Three-dimensionally preserved Ediacaran fossils occur within globally distributed sandstone beds. Sandy mass flow deposits of the Ediacaran Wood Canyon Formation in the Montgomery Mountains, Nevada, contain two different examples of erniettomorphs, soft-bodied organisms with uncertain taxonomic affinities. One type exhibits mm-scale ridges, the other one is flattened and lacks any smaller diagnostic features, including a distinct lower boundary. We explore the preservation of both fossil types by petrography, Raman and X-ray spectroscopy and X-ray diffraction. All fossils and the surrounding sediments contain quartz grains, iron-rich chlorite, and muscovite. The ridged fossils contain about 70% larger quartz grains relative to the other fossil type, which suggests that the fossilized organisms lived at two different locations. Chlorite and muscovite in the fossils and the sediment likely originated from smectite and kaolinite precursors that underwent lower greenschist facies metamorphism. The inferred original abundances of kaolinite and smectite and the appearance of a continuous, distinct, clay- and kerogen-rich bottom boundary in the ridged fossil suggest that these clay minerals helped preserve the finer-scale features of the organism. However, the flattened appearance and the discontinuous

interface of the ridgeless fossil also point to the importance of quartz in three-dimensional preservation in sandstones and siltstones.

Background:

Three-dimensionally fossilized, yet unpyritized soft tissues, occur rarely in the fossil record within sandstone beds, but are notable during the late Ediacaran (1-4). These select taphonomic windows enable investigations of the potentially basal mMetazoan clades (5, 6). Cast-and-mold-style Ediacaran fossils found within globally distributed sandstone beds (2, 4, 7, 8) inspire numerous hypotheses about fossilization mechanisms such as pyritization (e.g.(4, 9-11)), silicification (e.g.(12, 13)) and aluminosilicification (e.g. (14)). The style of preservation can tell us about the surrounding environmental conditions and the original tissue types, i.e., factors used to assess the lifestyles, diversity of taxa and types of organisms during the latest Ediacaran (15-17)**.** Specifically, determining how different taphonomic windows preserve diagnostic characters directly informs interpretations of fossils on the basis of diagnostic characters (17-20).

The three-dimensional morphology of soft-bodied organisms can be preserved when the decay of soft tissues is delayed (21) and/or precipitated minerals replace the tissues (22, 23). Chemical and physical conditions during the early stages of decay can influence mineral precipitation and delay the decay of soft tissue. Anoxic conditions, which are known to occur around unburied (21) and buried (23) decaying tissues, may limit microbial activity and the decay of organic material (21). The abundance and composition of clay minerals within the sediment may additionally delay the decay (24), if the adsorbed or authigenic clay minerals protect organic matter from degradation (25-27). Taphonomy experiments have tested the role of quartz, calcite, kaolinite, and illite in delaying the decay of soft tissue (24, 28-30), but it is not known how mineral mixtures that are common in natural sediments preserve different tissues. A recent study reported the formation of clay veneers around muscle tissue buried in kaolinite (28). Illite,

kaolinite, and their metamorphic products are often associated with Ediacaran and Cambrian cast-and-mold fossil assemblages, but it is debated whether these were detrital or authigenic minerals present during the initial fossilization process, or formed later during metamorphism (e.g.(4, 14, 27, 31, 32)). Microbial reduction of iron and sulfate coupled to the organic decay is thought to have enabled the precipitation of sulfide minerals such as pyrite around Ediacaran fossils found in sandstone beds (22, 33, 34). However, it has been suggested that pyrite forms during later diagenesis and not during the initial decay of the organism (35). Although the presence of pyrite has only been directly observed in some fossil specimens (e.g.(2, 7, 11, 14)), some interpret iron oxides present within Ediacaran fossils as the result of pyrite oxidation (e.g.(36, 37)). A recent study supports the relationship between sulfide minerals and porous sandstones by showing that greigite, an iron sulfide mineral which forms in acidic environments, and iron oxides can precipitate on muscle tissues buried in quartz sand (28). Overall, the current uncertainties highlight the need to consider both early and late diagenetic pathways and metamorphism in fossil preservation (38).

Latest Ediacaran ~~The lower Wood Canyon Formation (WCF), located in the Montgomery mountains, Nevada, includes pristine~~ cast-and-mold-style and pyritized fossil assemblages have been discovered in the late Ediacaran to early Cambrian lower Wood Canyon Formation (WCF) in the Montgomery Mountains, Nevada ~~of the latest Ediacaran and the early Cambrian~~ (2). Muscovite and chlorite clay minerals are present throughout the lower WCF, indicating that this formation underwent lower greenschist facies metamorphism (39). The presence of cast-and-mold-style and pyritized fossils in the same formation offers an opportunity to reconstruct environmental conditions and the types of tissues that were preserved through analyses of mineral and organic distributions in the fossils and the surrounding sediment. The mass flow sandstone beds of WCF preserve two distinct cast-and-mold-style oval erniettomorphs: one with mm-scale ridges

and distinct lower boundaries, and one without these boundaries and ridges (2) (Figure 1). Here, we seek to reconstruct fossilization processes, microbe-mineral interactions, and conditions that preserved WCF erniettomorphs and address the origin of differences between the two fossil types. The mapped distributions of clay, oxide, and sulfide minerals and organic matter within and around the fossils reveal the potential roles of allochthonous clay minerals and authigenic mineral phases in the early stages of fossilization.

Materials and Methods:

Materials

Erniettomorph fossils were found within the lower Wood Canyon Fm. in the Montgomery Mountains, NV, and were previously described by Smith et al. (2). The erniettomorphs pictured in Figures 1b and 1c of this manuscript ~~is~~ are also shown in Figure 3d and 3i, respectively, of the previous study (2).

Methods

Thin sections + Petrography

The fossils analyzed were cut with a Struers Labotom-5 rock saw along the boxes indicated in Figure 1. Thin sections of these rock sections were prepared at Spectrum Petrographics (Vancouver, WA, USA). These thin sections were first viewed in transmitted and reflected light, under 2.5x, 10x, and 20x magnifications, using a Zeiss Axioscope A1 microscope equipped with a Zeiss AxioCam ERC 5s and ZEN imaging software. Scales in petrographic images were inserted using ImageJ (v1.52a) and any noteworthy features were annotated in Adobe Illustrator (vCS5). The photomosaics were created from transmitted light images taken at 2.5x magnification in Adobe Illustrator. Polished sections were also made of cross sections cut through the fossils. These sections were viewed with an AmScope stereo microscope equipped with a Am 3MP digital camera and

AmScope imaging software. The scale bars were added and the images were annotated in Adobe Illustrator.

Fifteen frames from each thin section photomosaic were chosen randomly and used for grain size analysis in ImageJ. Three 93,000 μm^2 areas were selected in each of the selected frames. A color threshold was optimized for each frame to select only the quartz grains. This threshold was then applied to the selected areas to measure the grain sizes and percent area occupied by the quartz grains. Each selected area was also assigned a placement in the thin section: *f* for areas inside the fossil, *I* for areas at the interface, and *o* for areas outside the fossil. The abundances of quartz grains in these regions were compared using independent t-test and ANOVA using the Numpy and Scipy.stats packages in Python 3. A levene test in scipy.stats package was conducted before ANOVA test to ensure that the data had equal variances. In cases where the ANOVA analysis showed a statistically significant difference, a Tukey HSD post-hoc analysis, which simultaneously compares means among all groups, was performed to find which regions had significantly different percent area of quartz from each other. This test was done with the statsmodels.stats.multicomp package in Python 3.

SEM/EDS

The thin sections were analyzed with the Supra 55VP FESEM at the Harvard University Center for Nanoscale Systems (CNS). The electron microscope was operated at an 8.5 mm working distance, with 200-400x magnifications, and a 2 keV accelerating voltage. The analyzed areas are marked by filled rectangles in the photomosaics shown in Figure 3. Because the thin sections were not coated, the working energy was tuned to minimize the charging effects. Energy-dispersive X-ray spectroscopy (EDS) of the same areas acquired spectra at a working distance of 8.5 mm and a beam energy of 12 keV. The spectra and map data were collected with the program EDAX Genesis (v6.54) available at the same facility.

XRD

The ridged erniettomorph thin section was mounted onto a xy stage with double-sided tape and analyzed by the Bruker D8 Gadds Multipurpose Diffractometer at the Center for Materials Science and Engineering at MIT. The spectra were collected as line scans indicated by the red dashed line in figure 3a. Each spectrum was collected for 8 minutes from 2θ values of 5 to 80 degrees over four frames using the Glancing Incident X-ray detector (GIXD). The orientation of the sample relative to the x-ray beam was optimized to reduce the scan area along the width of the fossil. This was done to differentiate between areas along the line scan of the fossil. The data collected was then imported into the Bruker Diffrac Eva software and converted into a 1-D scan. These 1-D scans were then analyzed using the HighScore Plus software commercially available from Malvern Panalytical.

Micro-XRD/micro-probe

The thin sections were analyzed with the micro-XRD and micro-probe beamlines at the Advanced Light Source at the Lawrence National Laboratory in Berkeley, CA (beamlines 12.3.2 and 10.3.2). Thin sections analyzed by μXRD were taped onto the XYZ stage and analyzed at beam energy of 8 keV. Each frame was collected for 30 seconds. Regions mapped in this manner are indicated by dashed rectangles in the photomosaic (Figure 3). The spectra of individual frames from each region were added using the XMAS software and integrated from 2θ values of 13 to 65 degrees over chi values of -30 to 30 to create a 1-D scan. These scans were analyzed in HighScore Plus to identify mineral phases.

Raman spectroscopy

Minerals and organic matter in thin sections were examined by the Hyperspectral Darkfield Raman microscope located in the CNS facility at Harvard. Excitation lasers at 785 nm and 405 nm were used and the Raman shifts were collected from 50 to 2200 cm^{-1} with a grating of 600gr/mm or

from 150 to 3200 cm^{-1} with a grating of 1800gr/mm for each wavelength. The spectra and maps were collected over 5-10 second intervals with 100% of the laser energy. The slit size was 100 micrometers and the hole size was 300 micrometers for both laser wavelengths. Spectra were analyzed using the KnowItAll software and mineral maps were then made in the LabSpec 6 software commercially available from Horiba Scientific.

Results:

Fossil morphology and appearance in hand samples

The erniettomorph fossils ~~occurred~~ were found in float within ~~the~~ sandstone and siltstone beds (Figure 1) and stood out from the surrounding sediments, likely due to differential weathering. The upper surfaces of both fossils weathered to a darker color relative to the interior sediments. Two morphotypes were evident in hand samples, both approximately 6 cm long and 3.5 cm wide, and had a similar ovoid shape. Mm-scale ridges and a possible suture line were apparent on the top surface of one morphotype, the other had no diagnostic features present. The ridgeless fossil appears flattened compared to the ridged fossils, as noted by Smith et al. (2). Bottom surfaces of the fossils were not apparent in the hand samples.

To look at the bottom surface of the samples, three polished sections of each morphotype were cut and analyzed (Figure 2). All polished sections of the ridged fossil showed a 1-3 mm relief with respect to the top surface and a distinct lower boundary that visually separated the 5-7 mm thick fossil from the surrounding rock (Figure 2 a-c). A grain size change and a dark mineral layer were apparent across the boundary upon visual and microscopic examination of polished sections. In contrast, the bottom boundary of the ridgeless fossil was discontinuous and only present in some of the polished sections. In areas where the top surface of the ridgeless fossil had a 1-3 mm higher relief compared to the surrounding rock, there was a visible dark bottom boundary (Figure 2 d-f). The thickness of this fossil in

areas where the boundary is visible, varied from 5 to 10 mm, but not measurable in other areas. Cracks within the polished sections ran parallel to the bedding outside of both fossil types, and followed the lower boundary of the ridged fossil, indicating a plane of weakness within the rock. To compare the mineralogy and understand the origin of differences seen within the polished sections of the fossils, we analyzed each fossil morphotype in thin section (Figure 3).

Minerals in fossils and the surrounding sediment

To characterize the composition and distribution of minerals in the fossil and surrounding sediments, we first analyzed the vertical thin sections through fossils using petrographic microscopy. Quartz grains were abundant both within and outside of the ridged fossils, but the sizes of these grains differed. Medium to coarse sand grains were present within the fossils and very fine to fine sand quartz grains were present outside the fossil (Figure 3a). In contrast, the quartz grain size in ridgeless fossils was very fine to fine throughout the thin section (Figure 3b). The quartz grains in the ridged fossil were moderately sorted and the quartz grains in the ridgeless fossil were well sorted. All quartz grains were sub-angular and did not show any evidence of quartz overgrowth that would indicate later precipitation of silica. The quartz grains in the ridged fossil were ~70% larger compared to those in the ridgeless fossil (p-value = 8.83e-08), but occupied statistically identical mean percent areas in the two thin sections (p-value = 0.12 for the test of statistically significant differences).

In ~~the~~ light of this difference in quartz grain sizes, we quantified the percent areas occupied by this mineral in the ridged and the ridgeless fossil. The clearly defined upper and lower boundaries of the ridged fossil enabled us to label the different areas used in the grain size and percent area measurements: within the fossil, at the interface, or outside the fossil. An

ANOVA analysis of the ridged fossil revealed statistically significant differences (p-value <= 0.0042 for all three comparisons) among the mean percent area of quartz grains in all three regions: this area decreased from 53% within the fossil to 39% at the interface to 25% outside of the fossil. The same method could not be applied to the ridgeless fossil morphotype, which lacked a clear interface. The average quartz area value of 53% within ridged fossil is higher than the average area of 33% within the entire thin section of the ridgeless fossil, and comparable to the maximum measured value of 54% within one frame of that fossil. Any differences in the area occupied by quartz grains translated directly into differences in the amount of clay minerals that occupied the spaces between the quartz grains.

Clay to silt sized grains with higher order birefringence in cross-polarized light (XPL) and minerals with a micaceous texture in plane-polarized light (PPL) filled all spaces between the quartz grains in both fossil types (Figure 4). These minerals followed the boundaries of the quartz grains, never cross-cut other grains and exhibited rather uniform elemental composition. These characteristics were consistent with the properties of allochthonous clay minerals. Potassium, iron, and magnesium were the major cations in the clay minerals (Figure 5), XRD spectra of the fossils identified these minerals as iron-bearing clinochlore and muscovite (Figure 6). The presence of chlorite and muscovite, respectively, matched the observed abundances of magnesium and potassium, respectively. Fe-XANES spectra of the ridged fossil also suggested that the valence of iron is Fe(II) and identified chlorite as the main iron-bearing phase (supplementary Figure 5). Kaolinite, a weathering product of clinochlore, was also evident from Fe-XANES of the surface of the ridged fossil (supplementary Figure 5).

Carbonates, sulfides, oxides and feldspars were present in both samples, but only as minor phases. Carbonate minerals were not evident from the petrographic images of the samples in either PPL or XPL or elemental maps of the fossils. X-ray diffraction spectra, however, showed the

presence of magnesian calcite and ankerite (Figure 6a). Sulfides and oxides were most noticeable as black mineral grains in transmitted light and as white-to-silver and yellow-to-gold colored minerals in reflected light (Figure 4). These minerals were sparsely distributed throughout the fossils and surrounding sediments and were not detected in the XRD spectra due to the low abundances. The sparsity of oxides and sulfides throughout the samples suggests that the reduction of sulfate and iron were not concentrated at the interface between the soft-bodied organisms and the surrounding sediments. All XRD spectra supported the presence of plagioclase and potassium feldspars throughout the samples (Figure 6). Common in siliciclastic sediments, these minerals accounted for the observed enrichments of calcium and sodium in some grains mapped by EDS.

Interface region/identification of fossil area

A continuous and visible lower interface separated the ridged fossil from the surrounding sediments., Aa dark, but a discontinuous interface was also observed in some cuts through the flattened, ridgeless specimens. This visible boundary between the ridged fossil and the surrounding sediment was defined partly by the differences in the grain size of quartz and in part by the presence of darker and finer-grained clay material that outlined ridges similar to those seen at the weathered top of the sample (Figure 2a). At this clay-rich lower boundary, the abundance of Al was similar to that in and outside of the sample, but the abundance of Si was lower (Figure 7), indicating the presence of a <10 μm thin layer that contained a different clay phase. At the same finer scale, EDS maps indicated the presence of a similarly thin layer of carbon in this region. Because the distribution of carbon there did not exhibit a spatial correlation with any of the other elements (Figure 7), we hypothesized the presence of carbonaceous material. Indeed, the Raman spectra collected from the carbon-rich areas near the interfaces contained the D and G bands characteristic for carbonaceous material (Figure 6 (40)). Other carbon-rich areas within the

ridged fossil were f~~au~~rther away from the interface outside of the fossil and were not associated with the changes in quartz grain size. The ridgeless fossil lacked equivalent petrographic distinctions, but a similar carbon-rich line appeared at two different depths within the thin section. The depth of one matched the depth of the lower boundary of the ridged fossil, the other one was much deeper and closer to the bottom boundary of the entire thin section (Figure 7).

Discussion:

The above-described compositional and morphological differences between the two erniettomorphs suggest potential differences in taphonomic processes. The precursor organisms of both fossils contained quartz grains and were buried by sediments that contained angular quartz grains. Erniettomorphs from other localities are described as sand-filled soft and hollow saclike structures (e.g.(19, 41)). Similarly, the grains within the fossils from WCF must have been present within the organisms before burial. Quartz grains present within the ridged WCF fossils are comparable in size to the fine to coarse grains seen within Nama group cast-and-mold fossils (3, 4). The larger quartz grain sizes found in the ridged WCF fossil suggest that its precursor organisms lived in a more energetic area relative to the ridgeless fossil. The abundant chlorite and muscovite within and outside of the fossils also show that their precursors were present both in the original organisms and sediments that buried them. Because the WCF experienced lower greenschist facies metamorphism, the original clay minerals in and around the organisms were likely a mixture of kaolinite and smectite (42, 43).

Abundant detrital clay minerals in both samples are consistent with the hypothesized roles of clay minerals in the formation of cast-and-mold-style Ediacaran fossils (14, 24, 28, 31). For example, authigenic and adsorbed clay minerals form veneers that are thinner than 100 µm around muscle tissues buried in pure kaolinite, whereas discontinuous greigite and iron oxides precipitate within tissues buried in sand. Thus, the formation of early

diagenetic minerals requires microbial activity and the associated pH changes and appears to depend on the composition of the surrounding sediment (28). At this point, it is not entirely clear which features and early diagenetic minerals to expect in clay/sand mixtures. Continuous, thin layers of authigenic and detrital clay minerals are present at the lower boundary of the ridged fossils and may have been originally present at the now weathered surface. The observable enrichment of carbonaceous material at this fossil-sediment interface suggests that the clay minerals at the interface preserved some carbonaceous material during organic decay and early diagenesis. At the same time, the lack of a continuous visible lower interface in the ridgeless fossil suggests that the formation of clay-organic interfaces is key to preserving the three-dimensional features of soft-bodied organisms in clay-rich sandstones and siltstones. Selective preservation of organic matter associated with detrital or authigenic clay minerals has also been proposed for the Burgess Shale fossils (27). However, in contrast to the Ediacaran sandstones and siltstones that preserved erniettomorphs, the Burgess Shale-style preservation of reflective organic films occurred in fine clay matrixes that lacked larger quartz grains.

Pyritization and silicification have been suggested as fossilization mechanisms for erniettomorphs and cast-and-mold fossils at other localities (e.g. (11, 13, 14)). Pyritized fossils of tubular ~~organisms~~ body fossils have been reported in other shale, siltstone, and sandstone beds within the WCF (2) and the correlative Deep Spring Formation (Smith et al., 2016, Geology), but WCF erniettomorphs do not present evidence for either pyritization or silicification (2). If pyrite or other iron sulfide minerals were to have precipitated on the decaying walls of sand-filled organic sacs, these minerals or their oxidized weathering products should be concentrated at the fossil walls as the sites of localized microbially mediated iron and sulfate reduction (37, 44, 45). Instead, because sulfides and oxides were sparsely present throughout both samples and the surrounding sediments, it is unlikely that

microbial sulfate and iron reduction were confined to the organic walls only. Also, the lack of microbial structures within the fossiliferous sand channels (2) and in hand samples also does not support a direct role for sulfate- and iron reducing microbes in early fossilization (37, 44, 45). Sparsely distributed iron sulfide and oxide minerals are reported during the delayed decay of muscle tissues in sand (28), therefore, the same minerals may have formed during the decay of sand-filled erniettomorphs to be preserved as minor phases in micaceous sandstones. However, the presence of the pyritized tubular fossils within similar deposits suggests that the types of tissues the precursor organism had can control the taphonomic process which occurred.

In contrast to the WCF erniettomorphs, three-dimensionally preserved erniettomorph fossils from the Nama Group are found within pure quartz sediments (4, 46). In spite of the low abundance of clay minerals there, the Nama fossils preserve fine features at a similar scale to the ridges of the ridged WCF fossil. However, these fossils appear to be thicker than the WCF fossils analyzed here. Although the association of clay minerals and Ediacaran soft-bodied fossils has been described before (14, 31, 47), the processes controlling the formation of two-dimensional versus three-dimensional fossils and the preservation of mm-scale features and potential suture lines (e.g.(2, 4, 13, 14)) have not been fully explored. Clay minerals are known to inhibit or limit the microbial activity (24, 28) and help preserve organic compounds and fossils of soft-bodied organisms (e.g.(27, 48)). With this in mind, the poor preservation of diagnostic features in the ridgeless fossil are surprising, because its precursor organisms contained more clay and were buried in sediments that contained more clay minerals relative to the ridged fossil. This is consistent with a recent study that reported the flattening of muscles buried in kaolinite (28). Hence, we hypothesize that the different abundances of clay minerals within and around the fossils account for some of the morphological differences between the two erniettomorph fossil types in the WCF, as well as the differences between the WCF fossils

and erniettomorphs from other localities. The sand-filled interiors of the organisms, which would resist flattening compared to an organism filled with clay (28), may have enabled the three-dimensional preservation of erniettomorphs. Understanding the taphonomic process is critical to hypothesize about the diversity of species and tissue types present. In addition to the differences in the preservation quality between the ridged and the ridgeless fossils, they also may have had different precursor organisms. Taphonomy experiments that elucidate the role of different clay minerals in the early stages of fossilization, and in mixtures of clay minerals and quartz, can address these questions and help develop a better understanding of the conditions conducive to fossilization and the preservation of different tissues and diagnostic characters.

Conclusion:

Abundant quartz grains and clay minerals in erniettomorph fossils from the lower WCF and their distribution within and outside of the fossils of soft-bodied organisms in Ediacaran sandstones and siltstones had a role in fossil preservation. Angular quartz grains and the original clay minerals, kaolinite and smectite, filled the interiors of erniettomorph precursor organisms and the enclosing sediments. Sand grains maintained the macroscopic three-dimensional morphology of the organisms during decay, but evidence for a similar contribution of the sparsely distributed iron oxides and sulfides is lacking. Clay minerals adsorbed onto the surfaces of organisms during the early stages of decay, delaying the decay of organisms and preserving carbonaceous matter in <10 μm organomineral interfaces that separated the decaying organisms and the surrounding sediment. Microbial activity also induced the formation of a thin layer of authigenic clays at the sediment-fossil interfaces. These boundaries weather differentially from the surrounding sandstone/siltstone and act as planes of weakness within the rocks. The later lower greenschist metamorphism altered kaolinite to chlorite

and smectite to muscovite and partially graphitized carbonaceous material within fossils and at the fossil-sediment interfaces. Although the morphological differences between the two erniettomorph fossil types may reflect original taxonomic differences between their precursor organisms, these observations may be due to purely taphonomic factors, such as the greater flattening in the presence of more abundant clay minerals. ~~Even though~~Although clay minerals are thought to help with preservation of finer scale feature, we propose that the abundance of quartz grains in Ediacaran sandstone deposits may ~~the~~ benefit the preservation of three-dimensional structures.

Acknowledgements

Funding

NSF EAR-#1827669 to EFS

Data, code, and materials

Competing interests

Authors' contributions

Figures

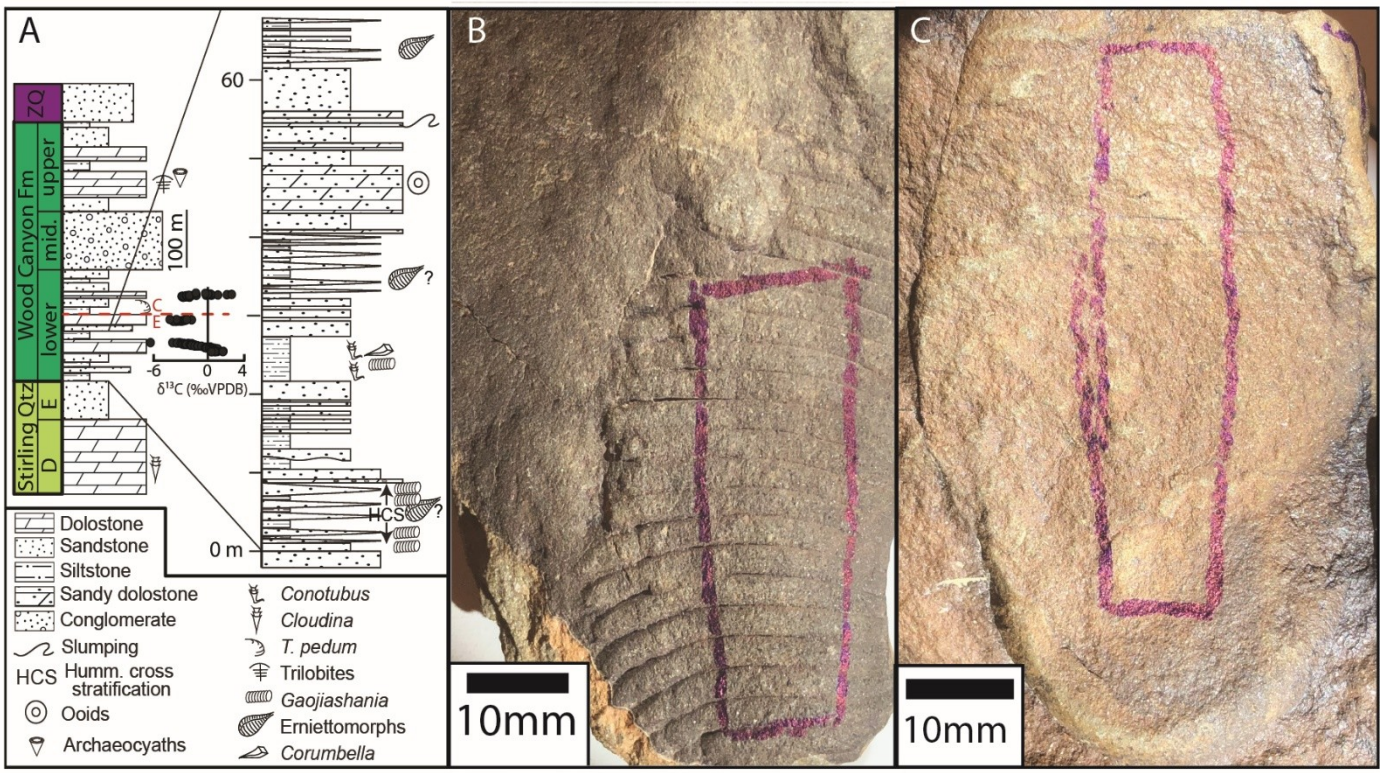

Figure 1. A) Stratigraphic section of the Montgomery Mountains, Nevada area from Smith et al., (2017). (B) Erniettomorph fossil with mm-scale ridges. C) Ridgeless erniettomorph fossils. The boxed regions show areas where the fossils were cut before thin sectioning and analyses.

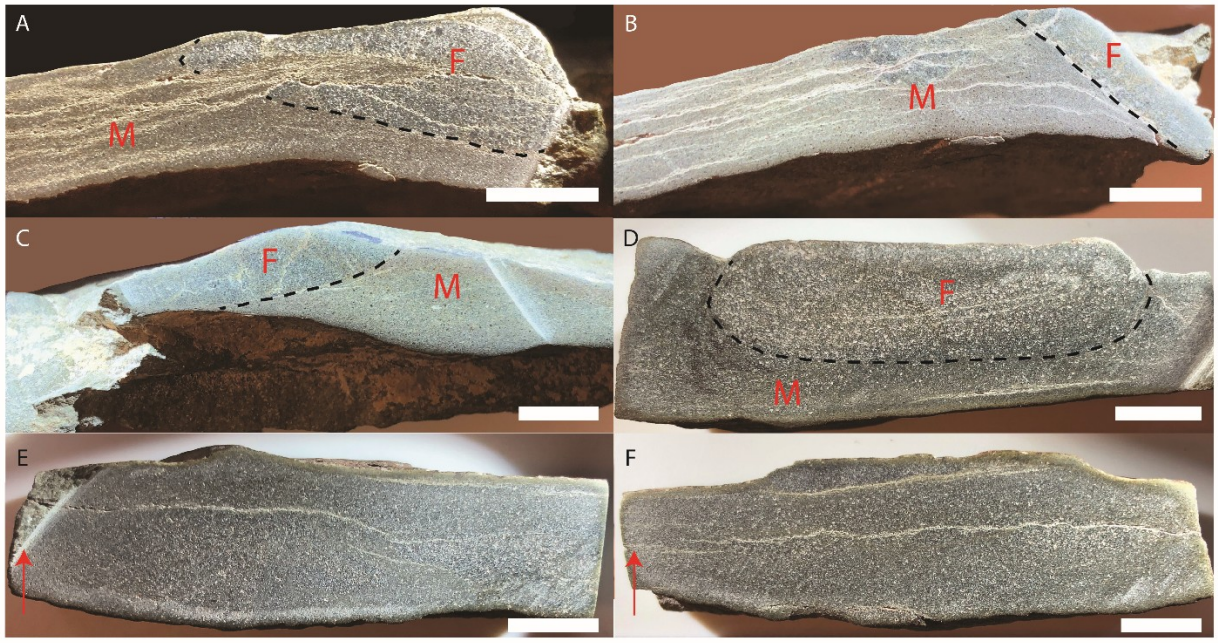

Figure 2. Polished cross sections through both fossil morphotypes. The ridged fossil (A-C) has a continuous interface while the ridgeless fossil (D-F) has a discontinuous interface. Black dashed lines indicate the interface between the fossil and surrounding rock. Arrows in E-F point towards the top of the fossil. Non-annotated polished sections are shown in supplemental Figure 1. F = fossil, M = matrix. Scale bars are 1cm.

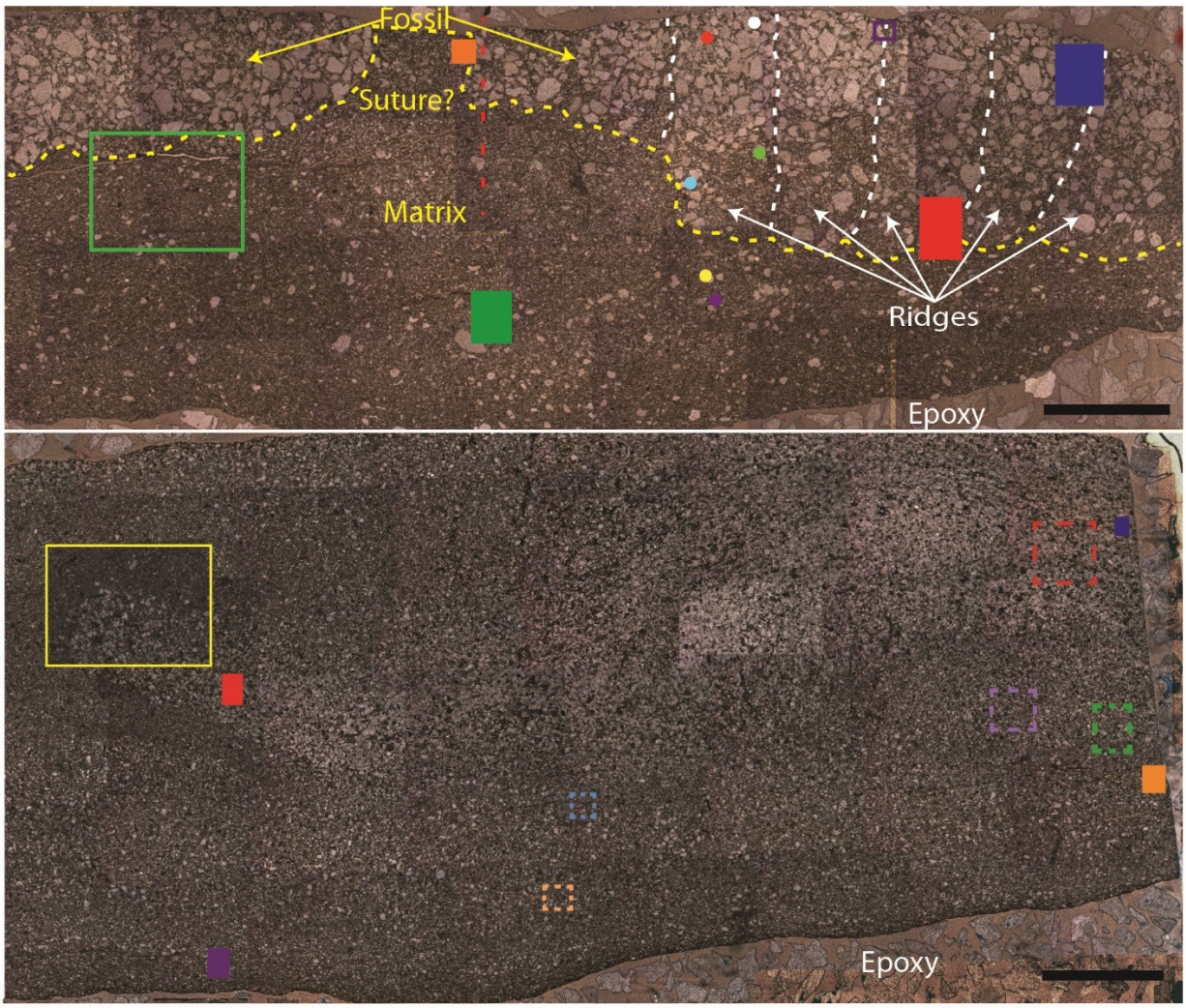

Figure 3. Photomosaics of the ridged (top) and ridgeless (bottom) erniettomorph fossil. ~~Top~~A) The ridged fossil is defined by medium to coarse angular quartz sand grains. The dashed yellow line follows the change from fine to very fine quartz grains that defines the interface between the fossil and the surrounding sediment. The dashed red line shows were the XRD line scan was taken. Darker mineral grains which follow the fossil ridges are also evident at the lower boundary. ~~Bottom~~B) The ridgeless erniettomorph fossil contains very fine to fine angular quartz sand grains and does not have a clearly defined lower or upper interface. The various colored shapes in both show areas that were analyzed by different

techniques. Non-annotated photomosaicc~~i~~s are shown in supplemental Figure 2. Scale bars are 3 mm.

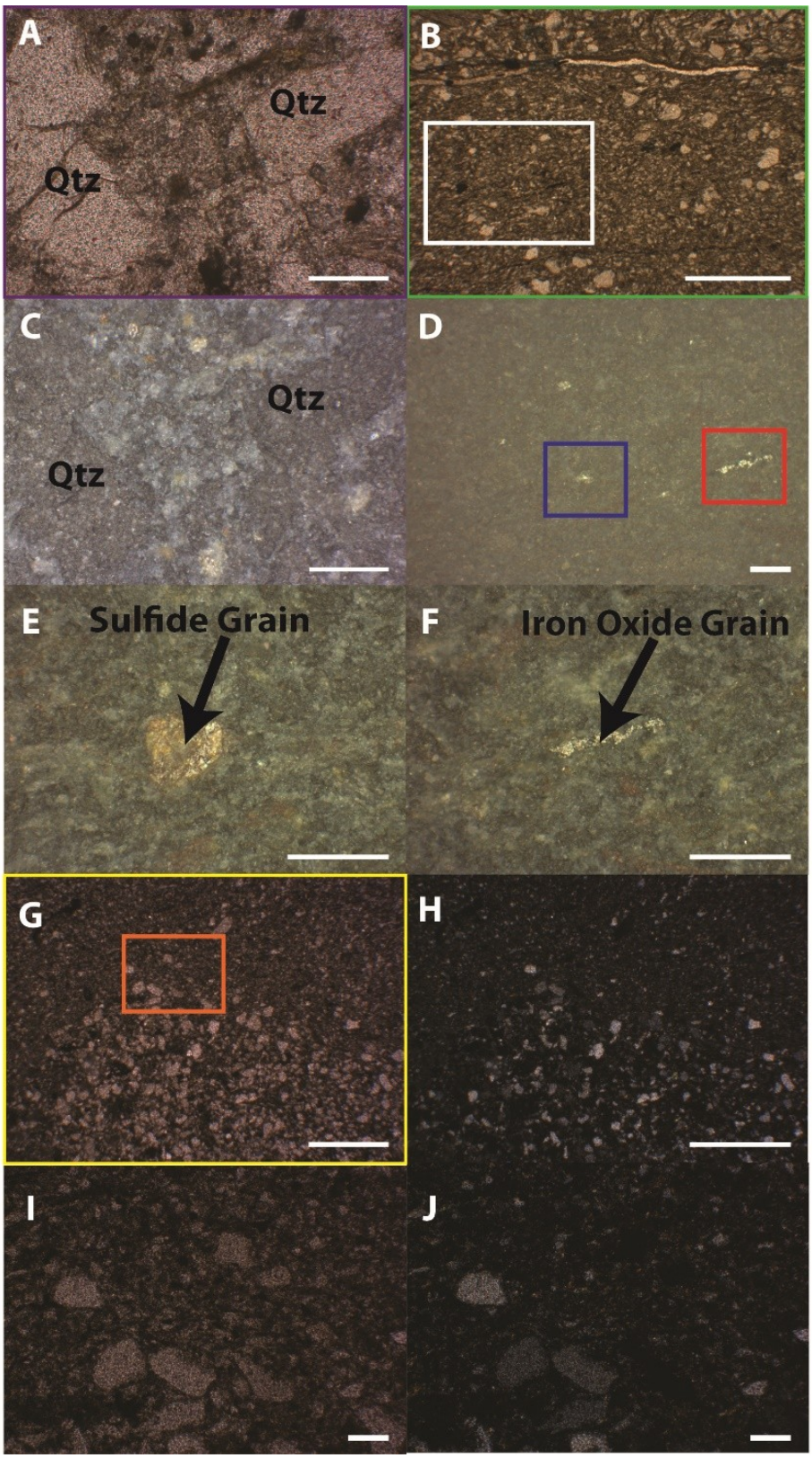
A
Qtz
Qtz
B
C
Qtz
Qtz
D
E
Sulfide Grain
F
Iron Oxide Grain
G
H
I
J

Figure 4. Photomicrographs of the ridged fossil (A-F) and the ridgeless fossil (G-J). Plane polarized transmitted light (A, B, G, I), plan polarized reflected light (C-F) and cross polarized transmitted light images (H, J)–. The areas shown in A, C, and G are identically colored rectangles (purple, green, yellow) within the photomosaics in Figure 3. E) and F) Sulfides and oxides, which are correlated to the blue and red boxes in D, respectively, are sparsely distributed throughout the sample. H) and J) Clay minerals in cross polarized transmitted light are more birefringent than surrounding quartz grains. Scale bar in C is 1 mm, and 100 micrometers for all others.

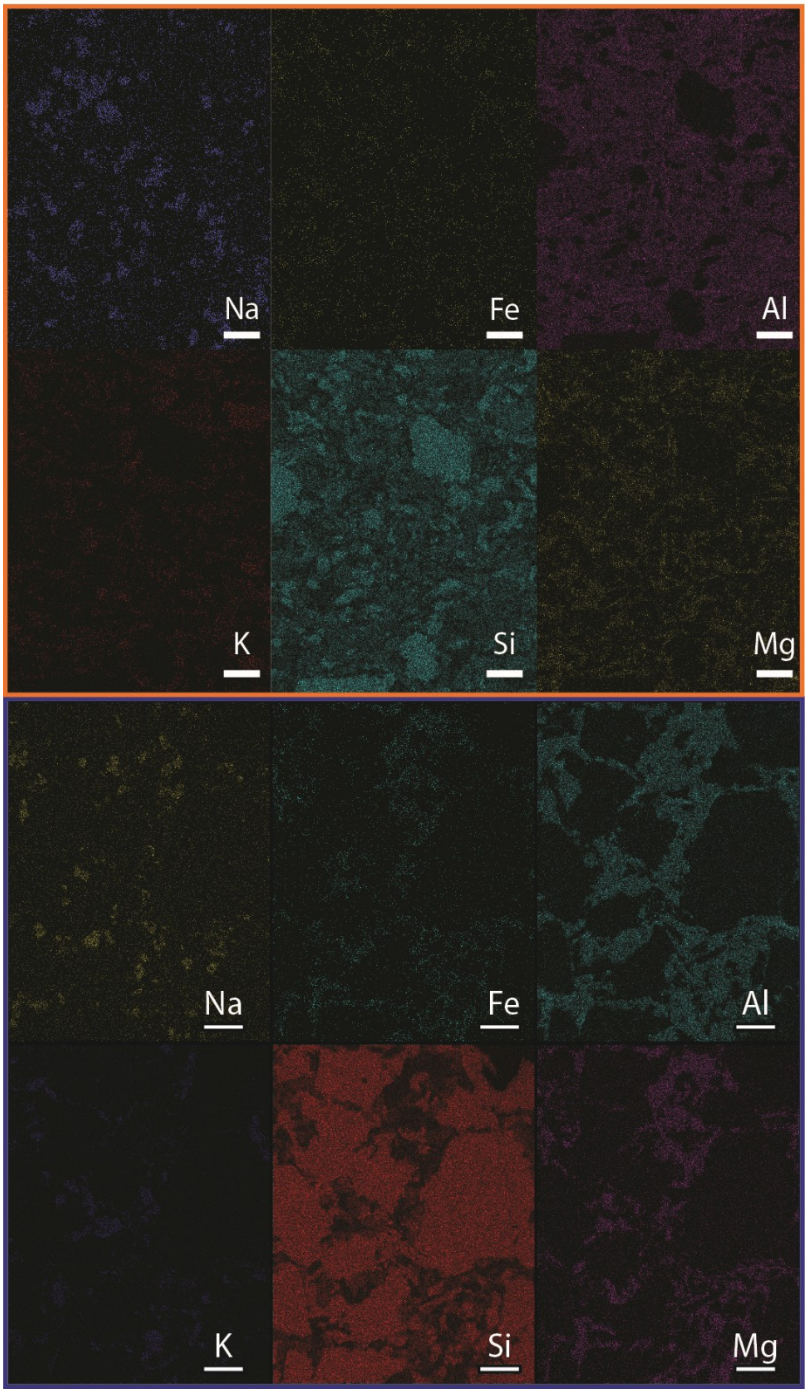

Figure 5. Representative EDS maps of the ridged fossil. All analyzed areas show abundant aluminosilicate minerals between quartz grains and most analyzed areas present no evidence for oxide or sulfide mineral grains. The compositions of the clay minerals are consistent with chlorite (Mg rich areas) and muscovite (K rich

areas). Similar patterns are seen within the ridgeless fossil EDS data (supplemental Figure 3). The color of the boxes (orange or blue) matches the color of the rectangles outlining the areas shown in the photomosaic in Figure 3a. Scale bars are 100 micrometers.

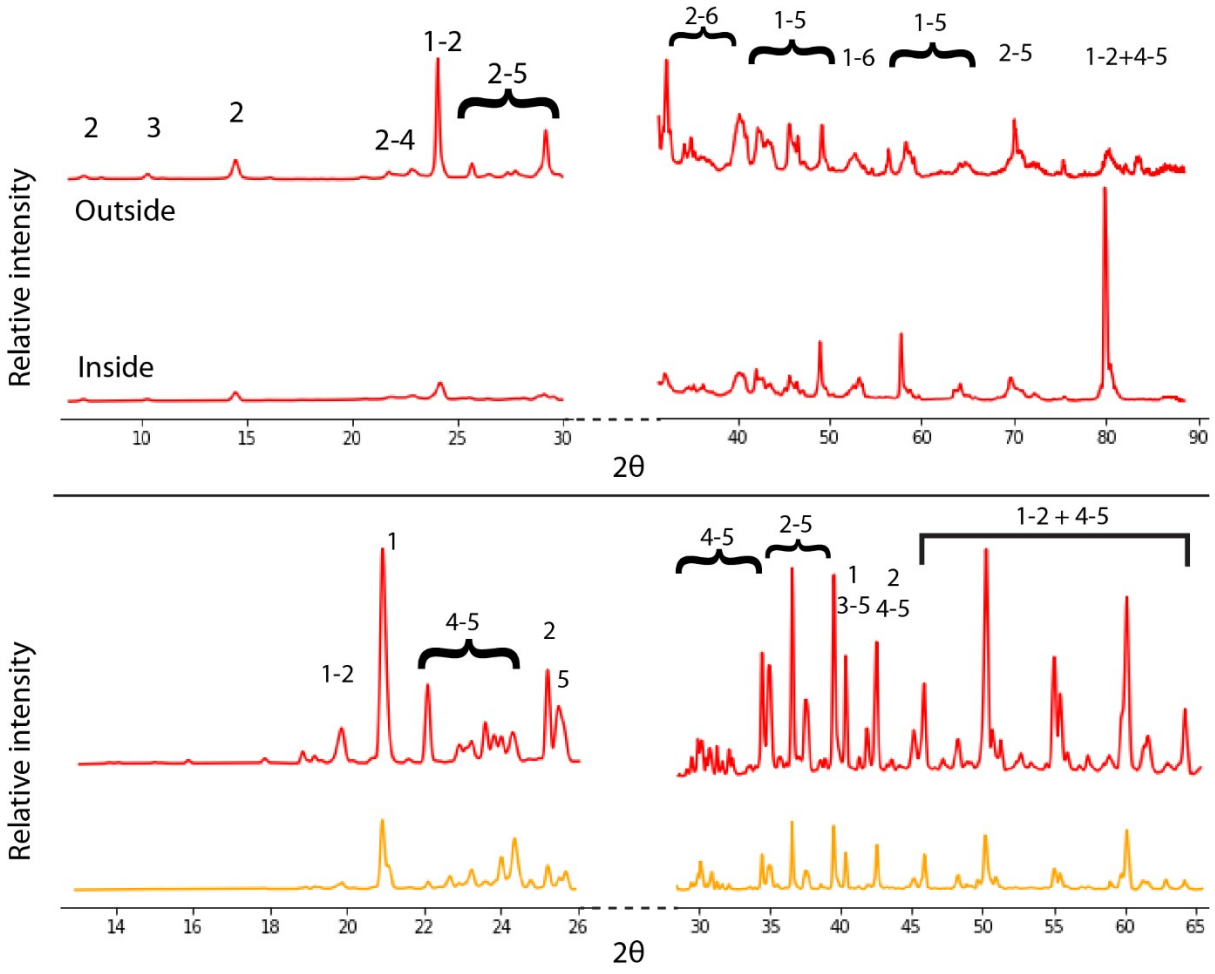

Figure 6. X-ray (top) and micro X-ray (bottom) diffraction patterns of the ridged and ridgeless fossil respectively. Two spectra from each morphotype were plotted since all spectra were similar. All other spectra are shown in supplemental Figure 4. (top) Spectra generated from a line scan across the ridged fossil, shown as the red-dashed line in the photomosaic in Figure 3a. These are labeled as wither being inside the fossil, or outside of the fossil. (bottom) 1-D micro-XRD scans of different areas in the ridgeless fossil, shown as unfilled rectangles of the same color in the photomosaic in Figure 3b Phases identified by XRD on both cross-sections are similar: (1) quartz, (2) clinochlore, (3) muscovite, an assortment of (4) plagioclase and (5) potassium feldspars, and (6) calcite/ankerite.

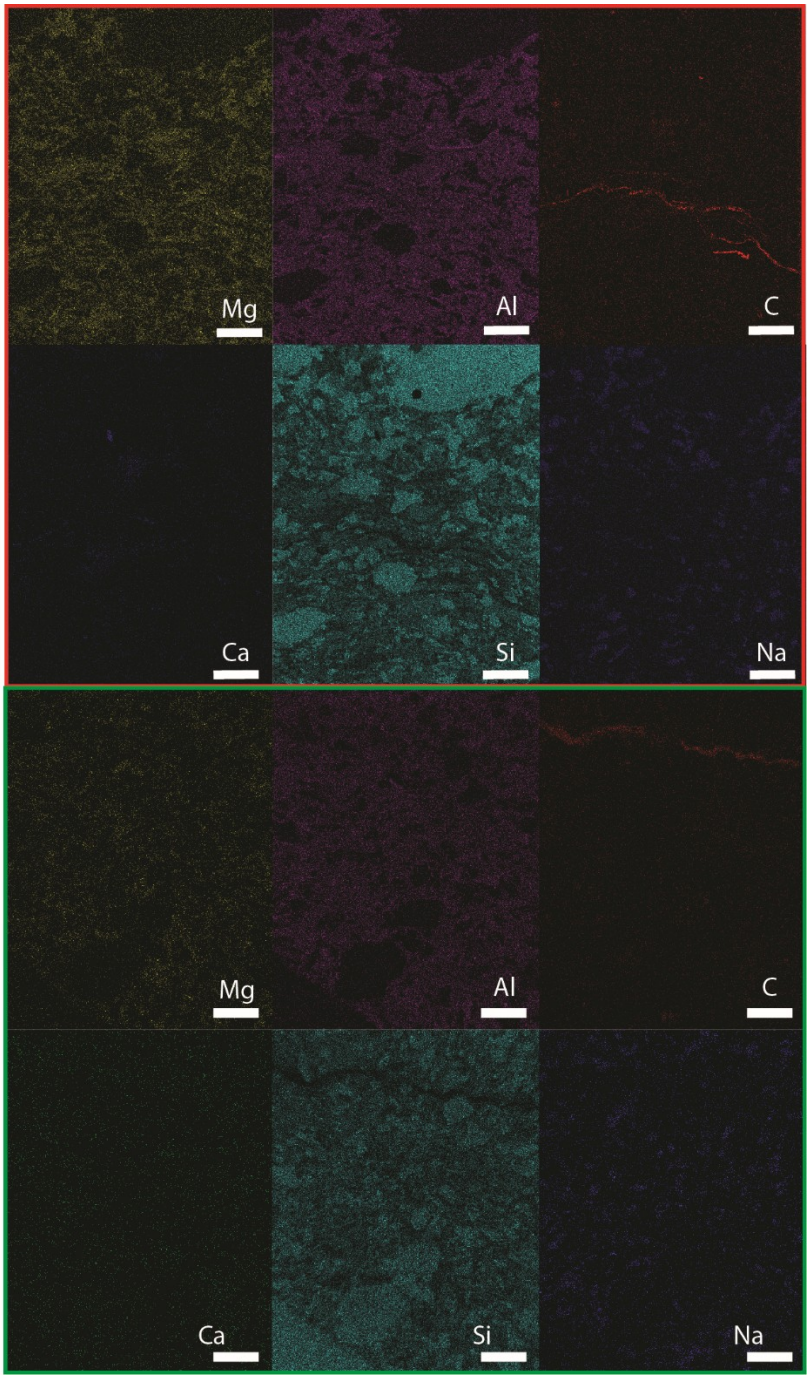

Figure 7. EDS maps of the carbon rich regions of the ridged fossil. Carbon enrichment occurs right at the change of quartz grain size (top) and in regions below this interface (bottom). This distribution pattern does not hold for the ridgeless fossil (supplemental Figure 6). The distribution of carbon does not correlate with the distribution of either magnesium or calcium in these regions. The

amount of Si decreases at the interface, the amount of aluminum remains consistent. The color of the boxes (red or green) matches the color of the rectangles outlining the areas shown in the photomosaic in Figure 3a. Scale bar in all images is 100 micronmeters.

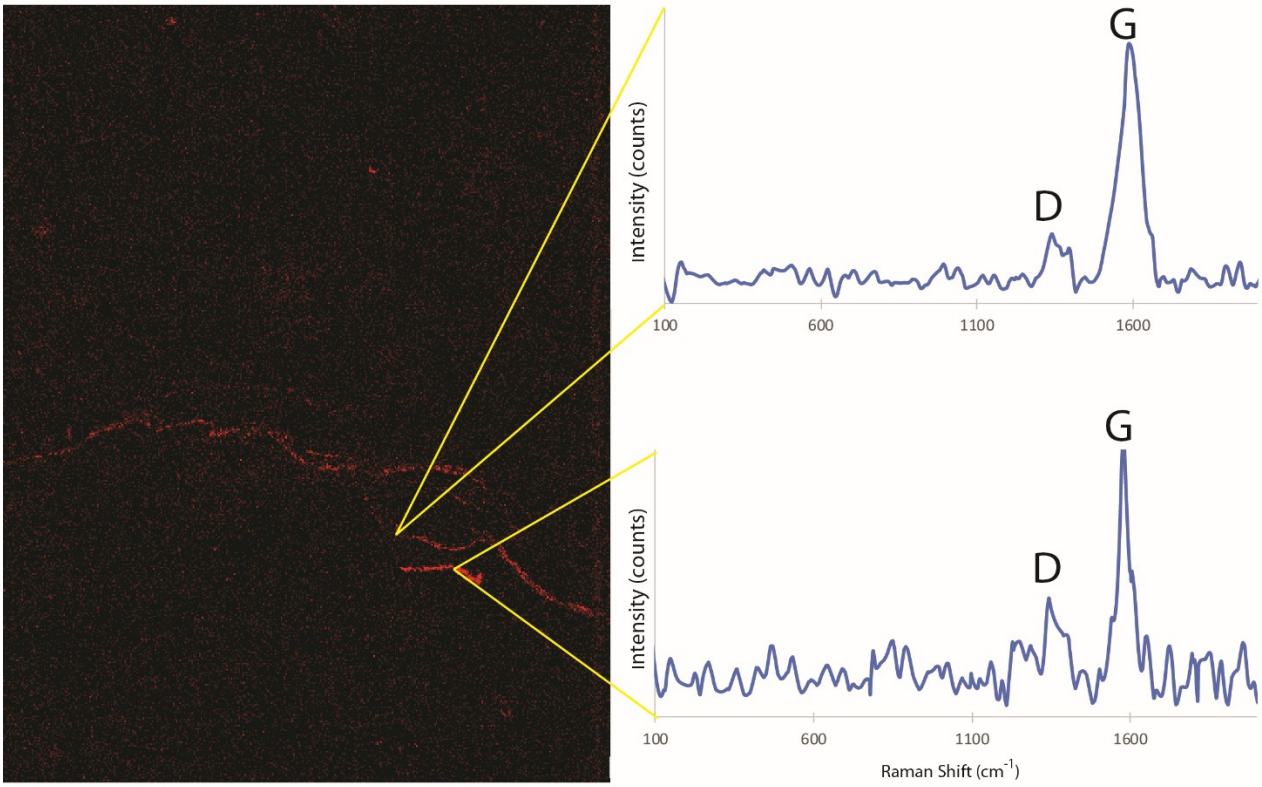

Figure 8. Raman spectroscopy of the carbon rich areas of the ridged fossil. These Raman spectra have the characteristic D and G band peaks of amorphous carbon. A similar pattern is seen in the ridgeless fossil (supplemental Figure 7). EDS image is the same as the panel labeled 'C' in the top boxed region of Figure 6. Scale bar is 100 micronmeters.

Supplemental Figures

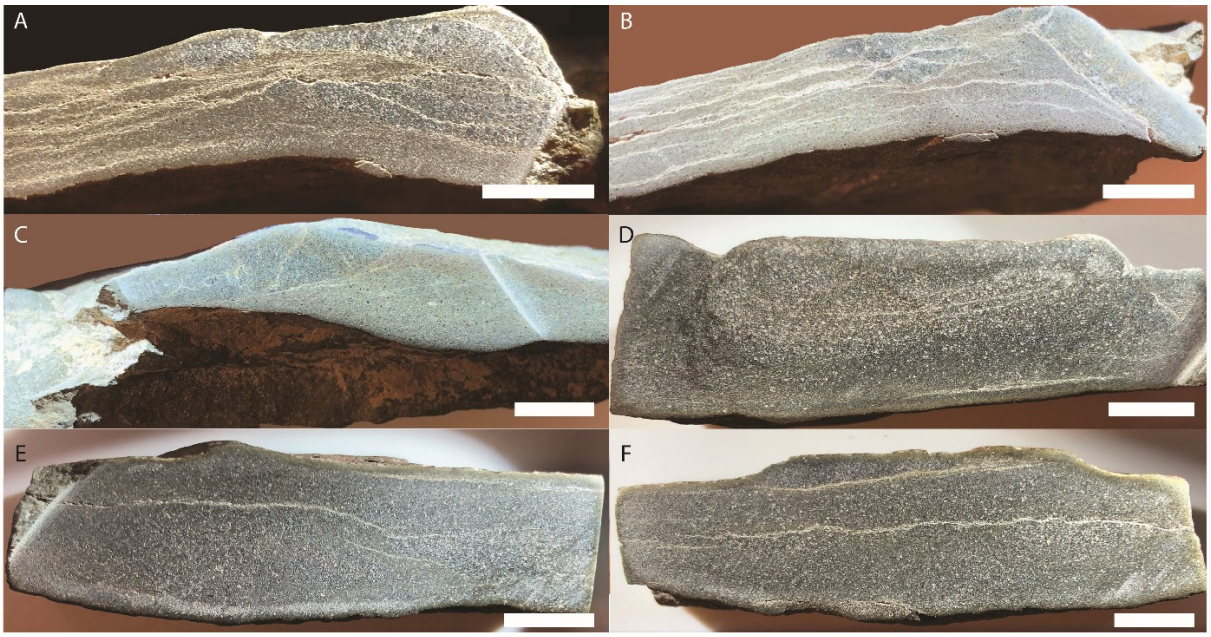

Supplemental Figure 1. Polished cross sections through both fossil morphotypes. The ridged fossil (A-C) has a continuous interface while the ridgeless fossil (D-F) has a discontinuous interface. Annotated polished sections are shown in Figure 2. Scale bars are 1 cm.

Supplemental Figure 2. Non-annotated photomosaics of the ridged (top) and ridgeless (bottom) erniettomorph fossil thin sections. Annotated photomosaics are shown in Figure 3. Scale bar is 3mm.

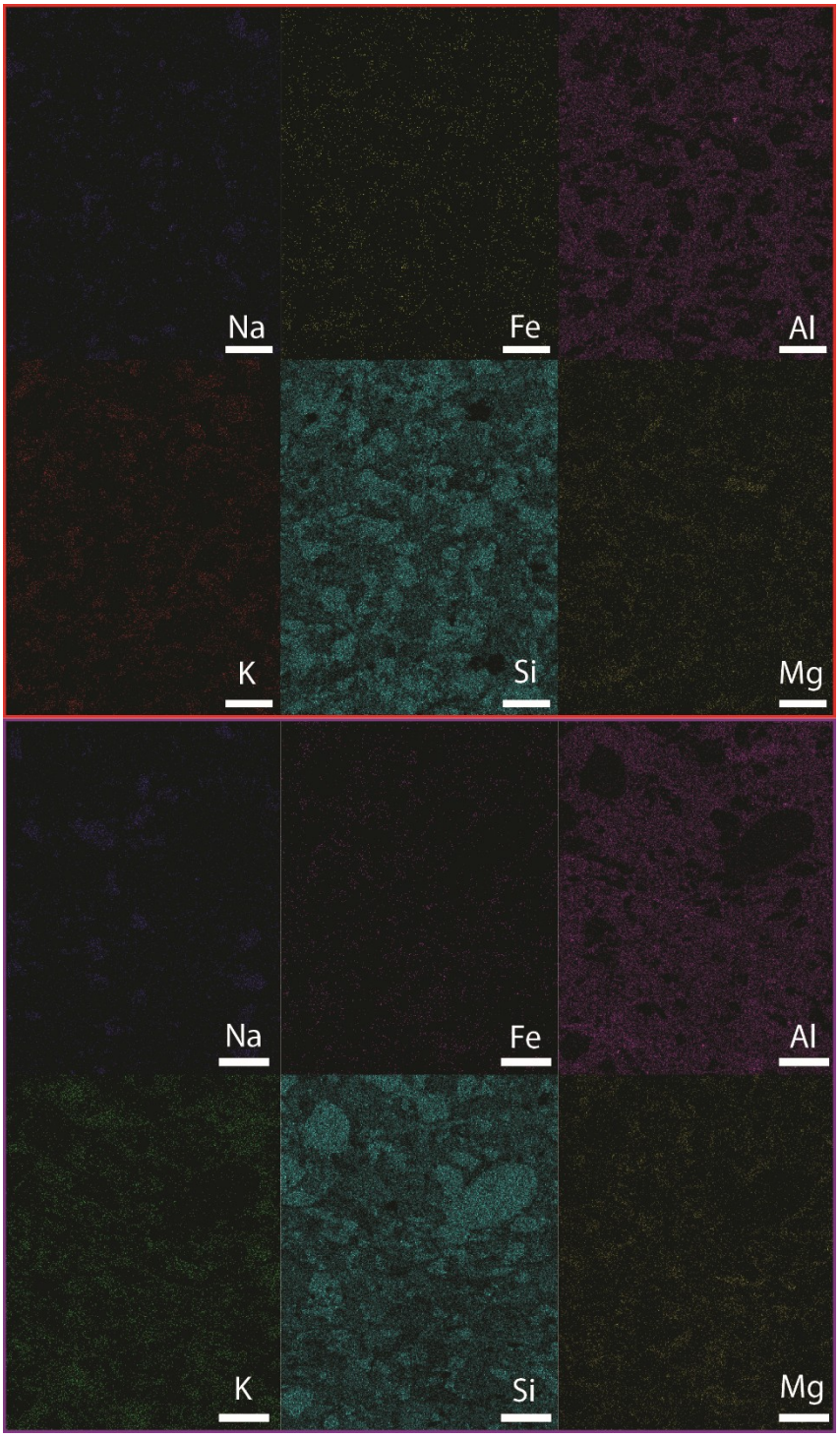

Supplemental Figure 3. Representative EDS maps of the ridgeless fossil. Similar patterns are seen within the ridged fossil EDS data (Figure 5). The color of the boxes (red or purple) matches the color

of the rectangles outlining the areas shown in the photomosaic in Figure 3b. Scale bars are 100 micrometers.

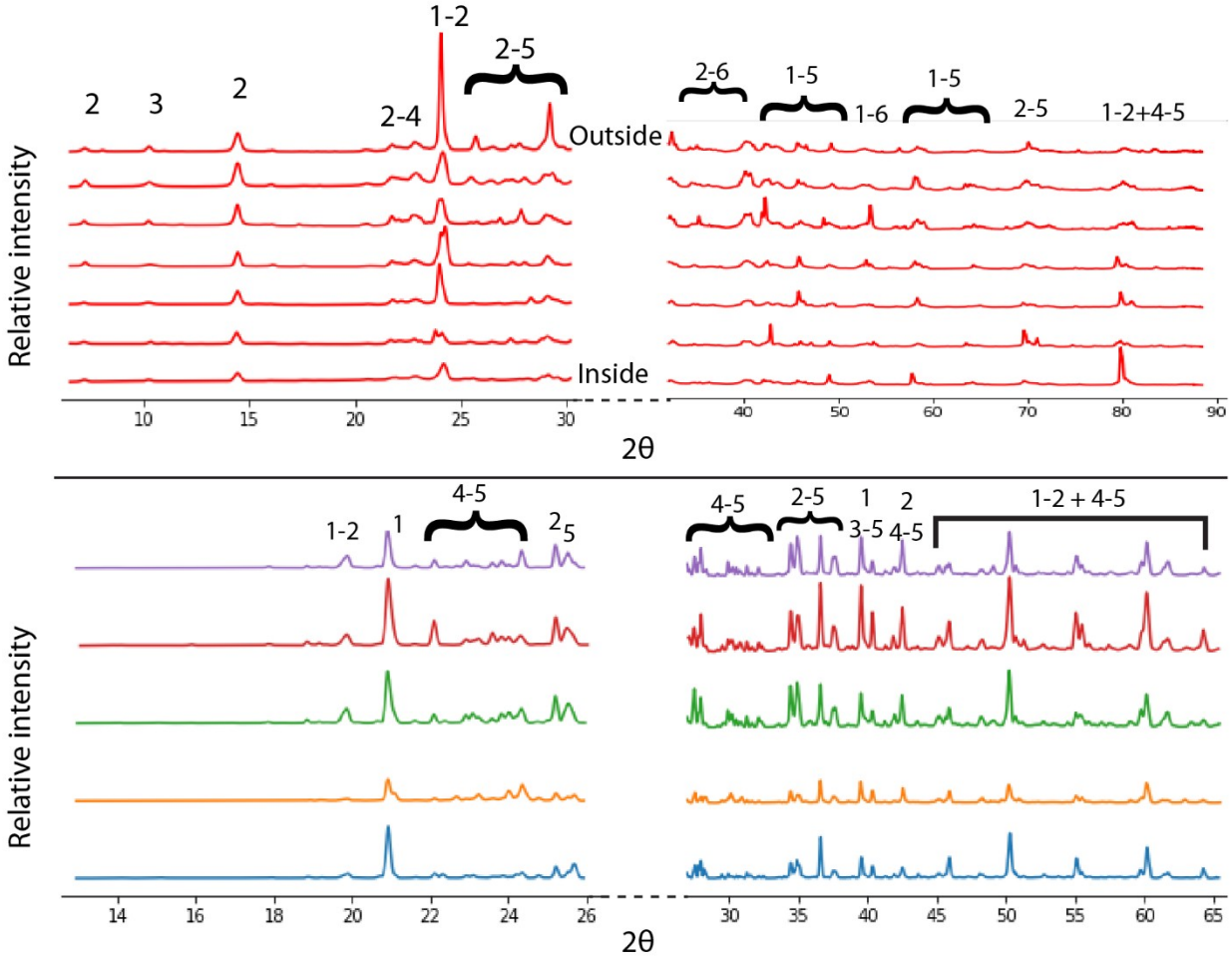

Supplemental Figure 4. X-ray (top) and micro X-ray (bottom) diffraction patterns of the ridged and ridgeless fossil respectively. (top) Spectra generated from a line scan across the ridged fossil, shown as the red-dashed line in the photomosaic in Figure 3a. These are labeled as wither being inside the fossil, or outside of the fossil. (bottom) 1-D micro-XRD scans of different areas in the ridgeless fossil, shown as unfilled rectangles of the same color in the photomosaic in Figure 3b Phases identified by XRD on both cross-sections are similar: (1) quartz, (2) clinochlore, (3) muscovite, an

assortment of (4) plagioclase and (5) potassium feldspars, and (6) calcite/ankerite.

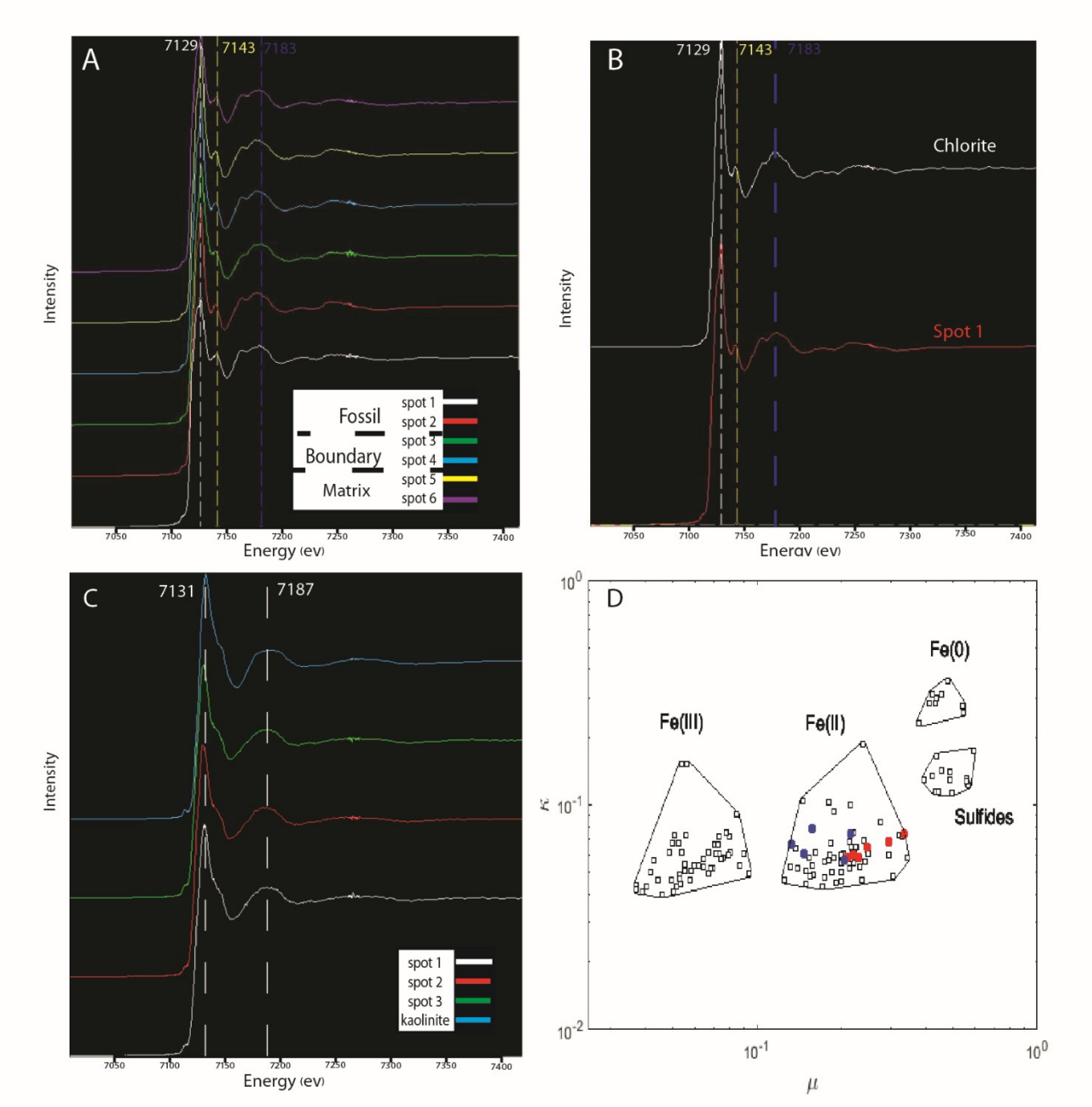

Supplementary Figure 5. Fe X-Ray Near Edge adsorption spectra (A-C) and Fe valence plot (D) generated from the ridged erniettomorph fossil. The color of the spectra lines in A correlate to the same

colored dots in 3a. B) These spectra look similar throughout the fossil, and match well with the chlorite standard from the beamline database. C) The points from the surface show the match well with kaolinite, a weathering product of chlorite. The valence plot also suggests that the form of iron in these samples (the blue and red dots) is Fe(II).

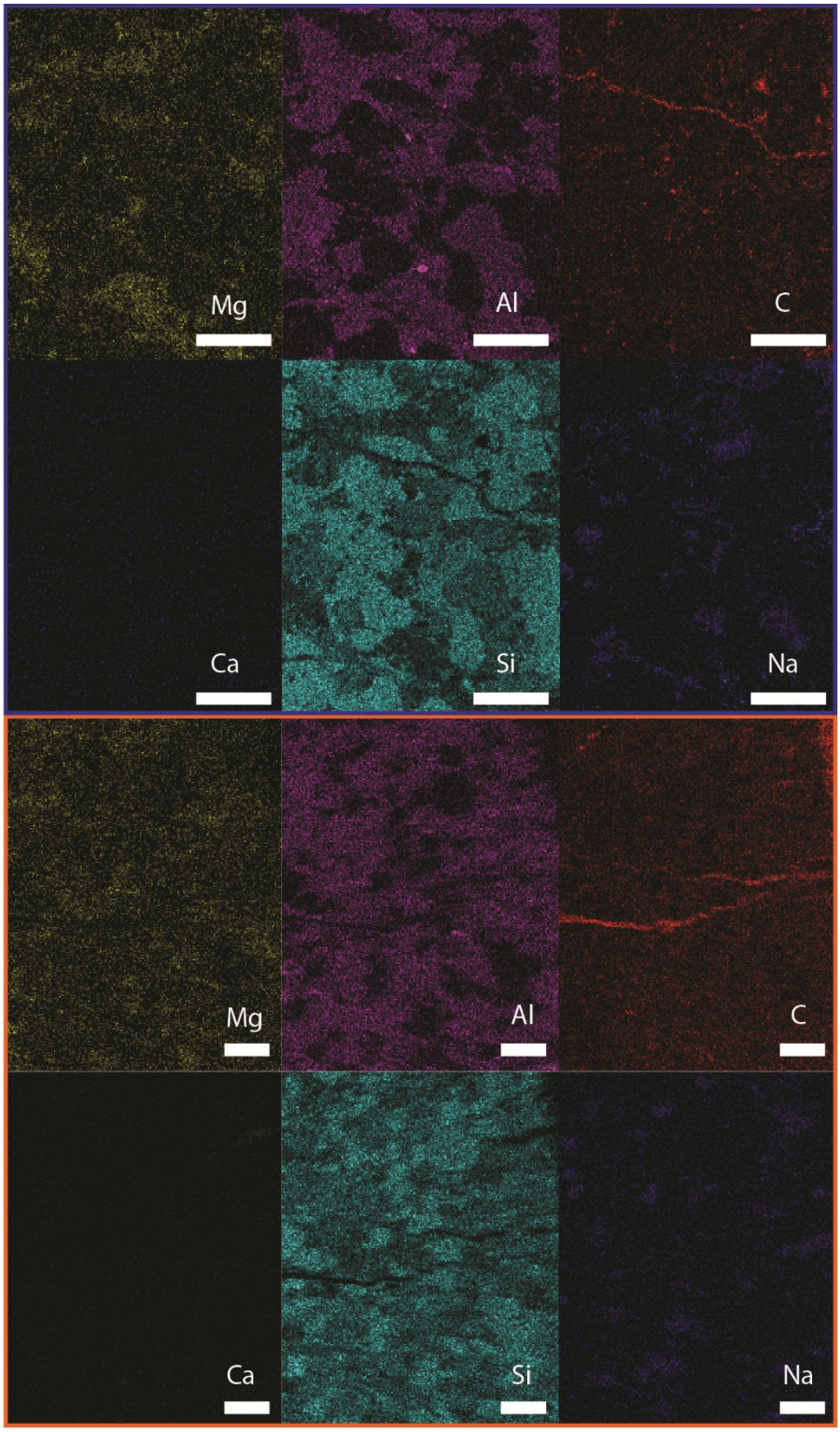

Supplemental Figure 6. EDS maps of the carbon rich regions of the ridgeless fossil. The distribution of carbon matched what is seen in the ridged fossil (Figure 7), however, the places where they occur

are not the same. The color of the boxes (blue or orange) matches the color of the rectangles outlining the areas shown in the photomosaic in Figure 3b Scale bar in all images is 100 micronmeters.

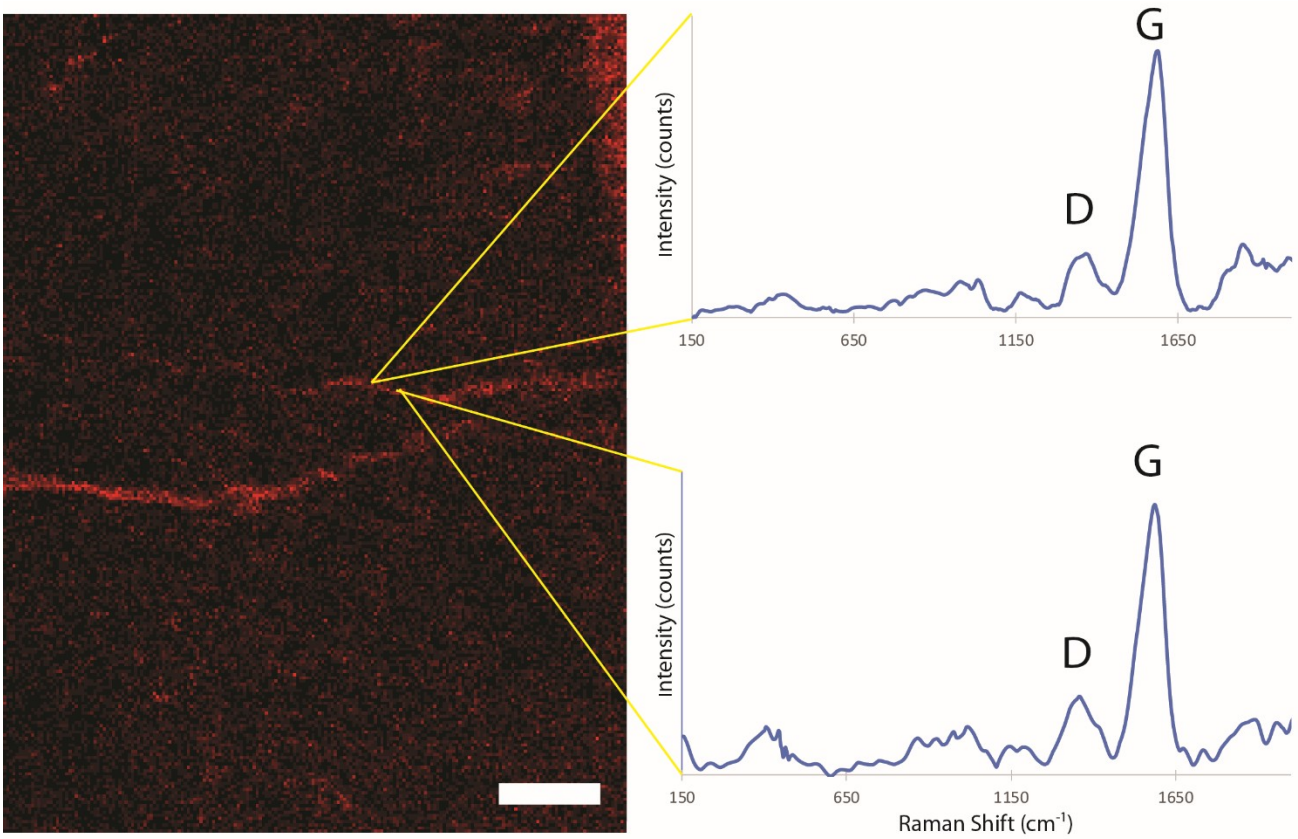

Supplemental Figure 7. Raman spectroscopy of the carbon rich areas of the ridgeless fossil. These Raman spectra have the characteristic D and G band peaks of amorphous carbon. Similar trends are seen in the ridged fossil (Figure 8). EDS image is the same as the panel labeled 'C' in the top boxed region of Supplemental Figure 5. Scale bar is 100 micronmeters.

1. Kenchington C, Wilby PR. Of time and taphonomy: preservation in the Ediacaran. Geological Society of America; 2014.

2. Smith E, Nelson L, Tweedt S, Zeng H, Workman JB. A cosmopolitan late Ediacaran biotic assemblage: new fossils from Nevada and Namibia support a global biostratigraphic link. Proceedings of the Royal Society B: Biological Sciences. 2017;284(1858):20170934.
3. Vickers-Rich P, Ivantsov AY, Trusler PW, Narbonne GM, Hall M, Wilson SA, et al. Reconstructing Rangea: new discoveries from the Ediacaran of southern Namibia. Journal of Paleontology. 2013;87(1):1-15.
4. Meyer M, Elliott D, Schiffbauer JD, Hall M, Hoffman KH, Schneider G, et al. Taphonomy of the Ediacaran fossil Pteridinium simplex preserved three-dimensionally in mass flow deposits, Nama Group, Namibia. Journal of Paleontology. 2014;88(2):240-52.
5. Droser ML, Gehling JG. The advent of animals: the view from the Ediacaran. Proceedings of the National Academy of Sciences; 2015. p. 4865-70.
6. Yuan X, Xiao S, Parsley RL, Zhou C, Chen Z, Hu J. Towering sponges in an Early Cambrian Lagerstatte: Disparity between nonbilaterian and bilaterian epifaunal tierers at the Neoproterozoic-Cambrian transition. Geology. 2002;30(4):363-6.
7. Smith E, Nelson L, Strange M, Eyster A, Rowland S, Schrag D, et al. The end of the Ediacaran: Two new exceptionally preserved body fossil assemblages from Mount Dunfee, Nevada, USA. Geology. 2016;44(11):911-4.
8. Glaessner MF, Wade M. The late Precambrian fossils from Ediacara, South Australia. Palaeontology. 1966;9(4):599-628.
9. Borkow PS, Babcock LE. Turning pyrite concretions outside-in: role of biofilms in pyritization of fossils. The Sedimentary Record. 2003;1(3):4-7.
10. Briggs DE, Raiswell R, Bottrell S, Hatfield Dt, Bartels C. Controls on the pyritization of exceptionally preserved fossils; an analysis of the Lower Devonian Hunsrueck Slate of Germany. American Journal of Science. 1996;296(6):633-63.
11. Schiffbauer JD, Xiao S, Cai Y, Wallace AF, Hua H, Hunter J, et al. A unifying model for Neoproterozoic–Palaeozoic exceptional fossil preservation through pyritization and carbonaceous compression. Nature Communications. 2014;5:5754.
12. Muscente A, Hawkins AD, Xiao S. Fossil preservation through phosphatization and silicification in the Ediacaran Doushantuo Formation (South China): a comparative synthesis. Palaeogeography, Palaeoclimatology, Palaeoecology. 2015;434:46-62.
13. Tarhan LG, Hood Av, Droser ML, Gehling JG, Briggs DE. Exceptional preservation of soft-bodied Ediacara Biota promoted by silica-rich oceans. Geology. 2016;44(11):951-4.
14. Cai Y, Schiffbauer JD, Hua H, Xiao S. Preservational modes in the Ediacaran Gaojiashan Lagerstätte: Pyritization, aluminosilicification, and carbonaceous compression. Palaeogeography, Palaeoclimatology, Palaeoecology. 2012;326:109-17.
15. Laflamme M, Darroch SA, Tweedt SM, Peterson KJ, Erwin DH. The end of the Ediacara biota: Extinction, biotic replacement, or Cheshire Cat? Gondwana Research. 2013;23(2):558-73.
16. Narbonne GM. The Ediacara biota: Neoproterozoic origin of animals and their ecosystems. Annu Rev Earth Planet Sci. 2005;33:421-42.
17. Xiao S, Laflamme M. On the eve of animal radiation: phylogeny, ecology and evolution of the Ediacara biota. Trends in Ecology & Evolution. 2009;24(1):31-40.
18. Seilacher A. Vendobionta and Psammocorallia: lost constructions of Precambrian evolution. Journal of the Geological Society. 1992;149(4):607-13.

19. Seilacher A, Grazhdankin D, Legouta A. Ediacaran biota: The dawn of animal life in the shadow of giant protists. Paleontological research. 2003;7(1):43-54.
20. Valentine JW. Dickinsonia as a polypoid organism. Paleobiology. 1992;18(4):378-82.
21. Briggs DE, Kear AJ. Decay and preservation of polychaetes: taphonomic thresholds in soft-bodied organisms. Paleobiology. 1993;19(1):107-35.
22. Briggs DE. The role of decay and mineralization in the preservation of soft-bodied fossils. Annual Review of Earth and Planetary Sciences. 2003;31(1):275-301.
23. Allison PA. The role of anoxia in the decay and mineralization of proteinaceous macro-fossils. Paleobiology. 1988;14(2):139-54.
24. McMahon S, Anderson RP, Saupe EE, Briggs DE. Experimental evidence that clay inhibits bacterial decomposers: implications for preservation of organic fossils. Geology. 2016;44(10):867-70.
25. Lagaly G. Clay-organic interactions. Philosophical Transactions of the Royal Society of London Series A, Mathematical and Physical Sciences. 1984;311(1517):315-32.
26. Mortland M. Clay-organic complexes and interactions. Advances in agronomy. 22: Elsevier; 1970. p. 75-117.
27. Orr PJ, Briggs DE, Kearns SL. Cambrian Burgess Shale animals replicated in clay minerals. Science. 1998;281(5380):1173-5.
28. Newman SA, Daye M, Fakra SC, Marcus MA, Pajusalu M, Sara B Pruss, et al. Experimental preservation of muscle tissue in quartz sand and kaolinite. Society for Sedimentary Geology; 2019. p. 437-51.
29. Wilson LA, Butterfield NJ. Sediment effects on the preservation of Burgess Shale–type compression fossils. Palaios. 2014;29(4):145-54.
30. Naimark E, Kalinina M, Shokurov A, Boeva N, Markov A, Zaytseva L. Decaying in different clays: implications for soft-tissue preservation. Palaeontology. 2016;59(4):583-95.
31. Anderson EP, Schiffbauer JD, Xiao S. Taphonomic study of Ediacaran organic-walled fossils confirms the importance of clay minerals and pyrite in Burgess Shale−type preservation. Geology. 2011;39(7):643-6.
32. Butterfield NJ, Balthasar U, Wilson LA. Fossil diagenesis in the Burgess Shale. Palaeontology. 2007;50(3):537-43.
33. Berner RA. Migration of iron and sulfur within anaerobic sediments during early diagenesis. American Journal of Science. 1969;267(1):19-42.
34. Petrovich R. Mechanisms of fossilization of the soft-bodied and lightly armored faunas of the Burgess Shale and of some other classical localities. American Journal of Science. 2001;301(8):683-726.
35. Tarhan L, Planavsky N, Wang X, Bellefroid E, Droser M, Gehling J. The late-stage “ferruginization” of the Ediacara Member (Rawnsley Quartzite, South Australia): Insights from uranium isotopes. Geobiology. 2018;16(1):35-48.
36. Liu AG. Framboidal pyrite shroud confirms the 'death mask' model for moldic preservation of Ediacaran soft-bodied organisms. Palaios. 2016;31(5):259-74.
37. Gehling JG. Microbial mats in terminal Proterozoic siliciclastics; Ediacaran death masks. Palaios. 1999;14(1):40-57.
38. Page A, Gabbott SE, Wilby PR, Zalasiewicz JA. Ubiquitous Burgess Shale–style “clay templates” in low-grade metamorphic mudrocks. Geology. 2008;36(11):855-8.
39. Stewart JH. Upper Precambrian and Lower Cambrian strata in the southern Great Basin California and Nevada. 1970.

40. McNeil DH, Schulze HG, Matys E, Bosak T. Raman spectroscopic analysis of carbonaceous matter and silica in the test walls of recent and fossil agglutinated foraminifera. AAPG Bulletin. 2015;99(6):1081-97.
41. Laflamme M, Xiao S, Kowalewski M. Osmotrophy in modular Ediacara organisms. Proceedings of the National Academy of Sciences. 2009;106(34):14438-43.
42. Frey M, Robinson D. Low-grade metamorphism: John Wiley & Sons; 2009.
43. Eberl D. Clay mineral formation and transformation in rocks and soils. Philosophical Transactions of the Royal Society of London Series A, Mathematical and Physical Sciences. 1984;311(1517):241-57.
44. Liu AG. FRAMBOIDAL PYRITE SHROUD CONFIRMS THE ‘DEATH MASK'MODEL FOR MOLDIC PRESERVATION OF EDIACARAN SOFT-BODIED ORGANISMSEDIACARAN TAPHONOMYA. G. LIU. Palaios. 2016;31(5):259-74.
45. Callow RH, Brasier MD. Remarkable preservation of microbial mats in Neoproterozoic siliciclastic settings: implications for Ediacaran taphonomic models. Earth-Science Reviews. 2009;96(3):207-19.
46. Elliott DA, Vickers-Rich P, Trusler P, Hall M. New evidence on the taphonomic context of the Ediacaran Pteridinium. Acta Palaeontologica Polonica. 2011;56(3):641-50.
47. Laflamme M, Schiffbauer JD, Narbonne GM, Briggs DE. Microbial biofilms and the preservation of the Ediacara biota. Lethaia. 2011;44(2):203-13.
48. Butterfield NJ. Organic preservation of non-mineralizing organisms and the taphonomy of the Burgess Shale. Paleobiology. 1990;16(3):272-86.